

# Testing the TPF Interferometry Approach Before Launch

E. Serabyn and B. Mennesson  
 Jet Propulsion Laboratory, MS 171-113  
 California Institute of Technology  
 4800 Oak Grove Drive  
 Pasadena, CA 91109  
 818-393-5243  
 gene.serabyn@jpl.nasa.gov

*Abstract*—One way<sup>1,2</sup> to directly detect nearby extra-solar planets is via their thermal infrared emission, and with this goal in mind, both NASA and ESA are investigating cryogenic infrared interferometers. Common to both agencies' approaches to faint off-axis source detection near bright stars is the use of a rotating nulling interferometer, such as the Terrestrial Planet Finder interferometer (TPF-I), or Darwin. In this approach, the central star is nulled, while the emission from off-axis sources is transmitted and modulated by the rotation of the off-axis fringes. Because of the high contrasts involved, and the novelty of the measurement technique, it is essential to gain experience with this technique before launch. Here we describe a simple ground-based experiment that can test the essential aspects of the TPF signal measurement and image reconstruction approaches by generating a rotating interferometric baseline within the pupil of a large single-aperture telescope. This approach can mimic potential space-based interferometric configurations, and allow the extraction of signals from off-axis sources using the same algorithms proposed for the space-based missions. This approach should thus allow for testing of the applicability of proposed signal extraction algorithms for the detection of single and multiple near-neighbor companions. Here the optical approach and the expected performance of the experiment are described. Interestingly, because of the small inner working distance possible with this approach, such a "nulling coronagraph" may be able to outperform classical coronagraphs in certain respects.

## TABLE OF CONTENTS

|   |   |
|---|---|
| 1. INTRODUCTION.....                        | 1 |
| 2. MEASUREMENTS WITH A ROTATING NULLER..... | 2 |
| 3. IMPLEMENTING A ROTATING NULLER.....      | 3 |
| 4. BASIC PERFORMANCE.....                   | 5 |
| 5. IMPROVED PERFORMANCE.....                | 6 |
| 6. THE ROLE OF THE SPATIAL FILTER.....      | 8 |
| 7. SUMMARY.....                             | 8 |
| REFERENCES.....                             | 8 |
| BIOGRAPHY.....                              | 9 |

<sup>1</sup> 0-7803-9546-8/06/\$20.00© 2006 IEEE

<sup>2</sup> IEEEAC paper #1078, Version 2, Updated Jan 15, 2005

## 1. INTRODUCTION

To enable the direct detection of faint companions very close to bright stars, the development of techniques such as coronagraphy on single-aperture telescopes, and nulling interferometry between multiple telescope apertures is required. However, nulling interferometry differs from normal long-baseline interferometry in one important respect - the need to maintain a null at a fixed phase implies that the complex visibility of the source brightness distribution is in general not directly accessible. Instead, what is easily measurable is the flux transmitted by the instantaneous fringe pattern, so that a direct Fourier inversion to the source plane is not possible. Instead, inversion by more indirect techniques such as cross-correlation is likely necessary [1].

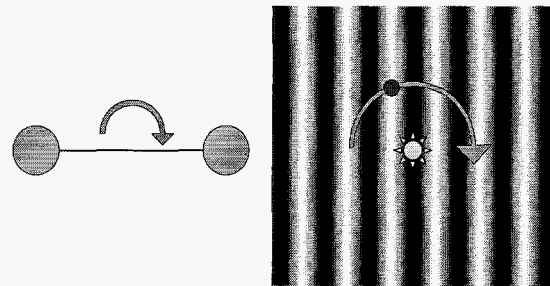


Figure 1. Schematic of a rotating long-baseline nuller and the accompanying fringe pattern. Destructive interference is maintained at the stellar position as the baseline and fringe pattern rotate. On the other hand, the off-axis companion's flux is modulated as the transmission fringes sweep past.

While image reconstruction with a nulling interferometer may be more indirect, the nature of the measurement is clear. As the nulling interferometer rotates, the nulling fringe pattern centered on the star [2] also rotates (Fig. 1). As it does so, the fringes sweep across the position of any off-axis companion, modulating its transmitted flux. At larger off-axis angles, more fringes cross the companion's

position, and so higher harmonics arise in the detected signal (Fig. 2). The harmonic content of the signal thus determines the companion's radial offset, and the azimuth of the transmission maximum determines its azimuth.

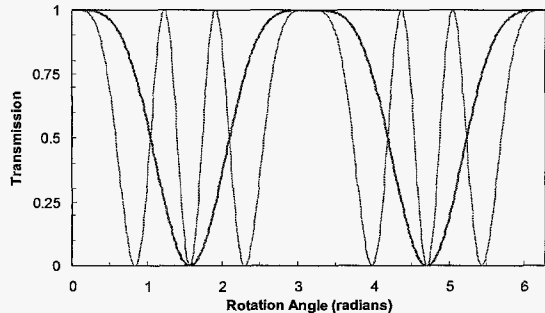


Figure 2. Signal from an off-axis source transmitted by a rotating single-baseline nuller. The thick green line is for a source at  $\lambda/2b$ , and the thin blue line for a source at  $3\lambda/2b$ . In both cases, the source is at zero azimuth.

Given the novelty of a rotating long-baseline nuller, and the ambiguity inherent in image reconstruction without full complex visibility data, it would clearly be very valuable to verify both the viability of the basic approach and the robustness of potential signal reconstruction algorithms by means of a ground-based demonstration prior to launch. Indeed in many areas, specification of instrumental parameters (even to the number of telescopes) will also be affected by a better understanding of such things as the reliability of image reconstruction algorithms. Such considerations led us to the idea of implementing a rotating nuller within the pupil of a single ground-based telescope, by establishing an interferometric baseline between separated sub-apertures within the common telescope pupil (Fig. 3). In the course of these considerations, it became clear that such an experiment would also provide a novel and potentially capable coronagraph. In the following, we describe the possible implementations and potential advantages of such an approach.

## 2. MEASUREMENTS WITH A ROTATING NULLER

Like any interferometer, a nulling interferometer will have a “fringe” response pattern on the sky. However, because of the need to keep a null fringe centered on the star, a normal scan in path length though a fringe (a fringe scan) to determine source visibilities is not possible. To elucidate the measurement approach while holding a null on the star, we begin with the source brightness distribution,  $S(\theta, \varphi)$ , a function of  $\theta$  and  $\varphi$ , the radial and azimuthal coordinates relative to the center of the star. In general,  $S$  includes both point source contributions from off-axis companions and extended contributions from both exozodiacal emission

around the target star and “background” emission, from e.g., our own solar system’s zodiacal disk. For simplicity, we assume monochromatic operation hereafter.

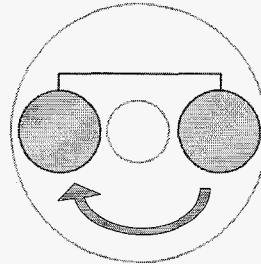


Figure 3. Rotating single baseline nuller (blue) within the pupil of a single-aperture telescope (gray outline). The light from the two sub-apertures is combined interferometrically in a nulling beam-combiner. The light from the area outside the sub-apertures is not collected.

We next define the instantaneous “nulled source brightness distribution,”  $S_N(\theta, \varphi)$ , as the product of  $S(\theta, \varphi)$  and the instantaneous fringe transmission pattern,  $T(\theta, \varphi, \alpha)$ . The function  $T$  depends on the configuration of apertures in the pupil plane, and, assuming spatial filtering of the focal-plane distribution, includes the coupling of the focal plane distribution to a single-mode fiber, which introduces a  $\theta$ -dependent transmission falloff. The function  $T$  then rotates with  $\alpha$ , the interferometer rotation angle. Explicitly,

$$S_N(\theta, \varphi) = S(\theta, \varphi)T(\theta, \varphi, \alpha). \quad (1)$$

The transmitted power detected after passage through a single mode fiber centered on the stellar image in the focal plane is the integral of  $S_N$  over the field of view:

$$P(\alpha) = \int S(\theta, \varphi)T(\theta, \varphi, \alpha) d\theta d\varphi. \quad (2)$$

The source distribution can then be reconstructed via e.g., cross-correlation [1], using

$$S(\theta, \varphi) = \sum P(\alpha) T(\theta, \varphi, \alpha), \quad (3)$$

where the sum is over rotation angle. In the simplest case of a single-baseline nuller, the fringe transmission is given by

$$T(\chi) = \sin^2(\chi/2) = (1 - \cos(\chi))/2, \quad (4)$$

where  $\chi$  is the relative phase between the two telescopes. For a given instantaneous orientation of the baseline vector,  $\mathbf{b}$ , and a point located at the vector angular position  $\theta$  in the fixed  $(\theta, \varphi)$  coordinate system on the sky,  $\chi$  is given by

$$\chi = \mathbf{kb} \cdot \boldsymbol{\theta} = kb\theta \cos(\varphi - \alpha). \quad (5)$$

This implies that the instantaneous fringe transmission pattern is given by

$$T(\theta, \varphi, \alpha) = (1 - \cos(kb\theta \cos(\varphi - \alpha)))/2. \quad (6)$$

The transmission vs. rotation angle is plotted for two radial offsets in Fig. 2, where the increased importance of higher harmonics at larger off-axis distances is evident.

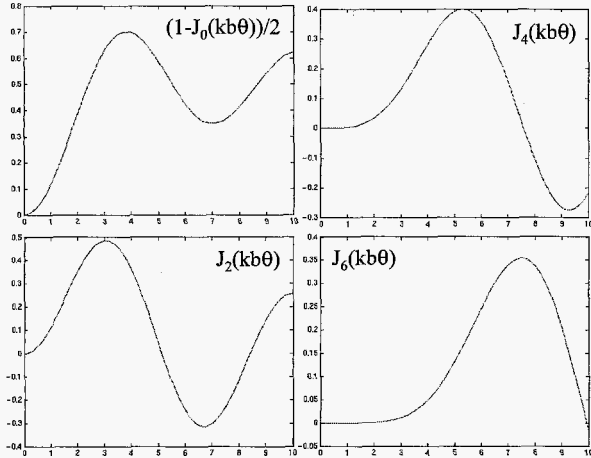


Figure 4. First four amplitudes in the harmonic expansion of the transmission of an off-axis companion by a single-baseline nuller, as a function of  $kb\theta$ . In these units, the first constructive fringe occurs at  $x = \pi$ . Interior to the first fringe maximum, most of the a.c. power is in the first harmonic at  $2\omega$ , while outside of that location, the higher harmonics quickly gain in strength.

To see this more explicitly, equation 6 can be expanded in a series of Bessel functions,  $J_n$ , of order  $n$ , as follows:

$$T(\theta, \varphi, \alpha) = (1 - J_0(kb\theta))/2 - \sum J_{2n}(kb\theta) \cos(2n(\varphi - \alpha + \pi/2)), \quad (7)$$

where  $n$  is summed from 1 to infinity. For a constant rotation rate,  $\omega$ , we have  $\alpha = \omega t$ , and the signal is seen to consist of a series of harmonics of the frequency  $2\omega$ . Figure 4 plots the amplitudes of the d.c. term and the first three harmonics as a function of  $kb\theta$ . For a source inside the first fringe maximum, the first harmonic dominates, but beyond that radius, higher harmonics increasingly contribute. It should thus be straightforward to verify this basic behavior with a ground-based rotating nuller well before the launch of any potential space-based nulling interferometer.

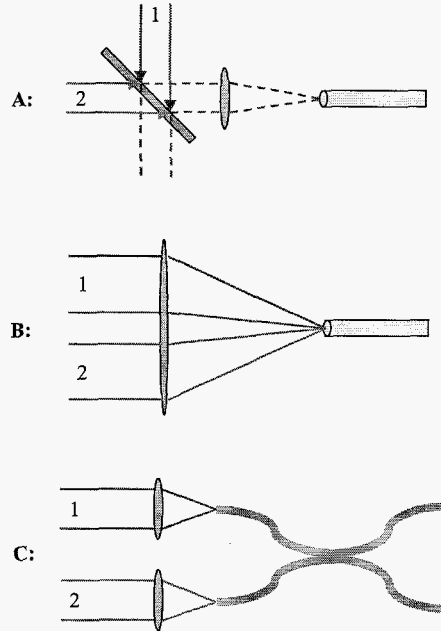


Figure 5. Schematic of the three possible types of nulling beam combiner. A: combination of beams at a beamsplitter. B: combination of beams at a fiber tip (the fiber nuller). C: combination by cross-coupling between fibers. In the fiber nuller, two spatially separated beams are focused onto a common single-mode fiber by a common optic. For all cases, a relative phase shift of  $\pi/2$  or  $\pi$  radians is applied by an achromatic phase shifter (not shown). In some cases, an achromatic  $\pi/2$  phase shift is also supplied by the beam combiner.

### 3. IMPLEMENTING A ROTATING NULLER

A number of different optical implementations might be used to define a set of sub-apertures within a telescope pupil, and to combine and null the beams. A number of general considerations guide the choice of specific implementation. First, maximization of sub-aperture areas and spectral bandwidth are desirable, in order to maximize the signal to noise (SNR) ratio, while maximization of the baseline length will yield the maximum angular resolution. However, one could in principle trade off sub-aperture diameter against a larger number of sub-apertures. In addition, a smaller sub-aperture size has the advantage of a larger single-mode field of view. It is also important to select an optical implementation that is simple, yet flexible and amenable to the introduction of path-length control schemes. In the following we concentrate mostly on the single baseline case to illustrate the issues, although multiple baseline cases are also possible.

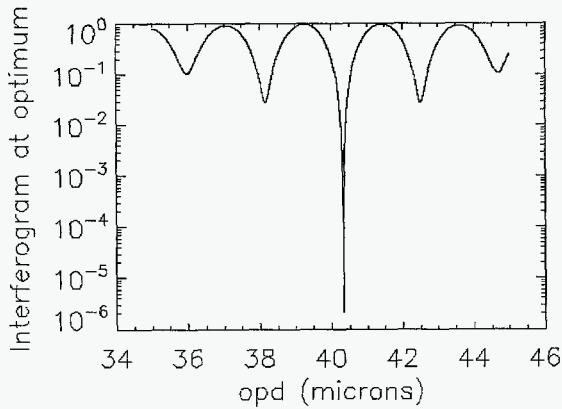


Figure 6. Null depths attainable with a  $\text{CaF}_2$  glass phase shifter in the K-band.

A number of different nulling beam-combination schemes can be used to null two beams, including classical beamsplitter-based systems, injection into a common fiber (the “fiber nulloer”), and cross-coupling between fibers (Fig. 5). The classical beamsplitter-based approach (Fig. 5; A) has a number of well known variants with one or two beamsplitters [3], and the fiber cross-coupler (Fig. 5; C) [4] tends to have dispersion issues. The relatively novel fiber nulloer (Fig. 5; B) is based on the injection of a number of beams into a common single-mode fiber in the focal plane [5,6]. Deep nulling of monochromatic light to close to the  $10^{-6}$  level has now been demonstrated with a fiber nulloer [6]. For more broadband nulling, an achromatic phase shifter to introduce a  $\pi$  radian phase shift between the two beams [7] is needed. Solutions for glass dispersion correctors are straightforward, and Fig. 6 shows a solution for  $\text{CaF}_2$  glass that produces deep nulls across the K-band ( $2.2 \mu\text{m}$ ). However, a fiber nulloer beam combiner has not yet been used for on-sky observations. In addition, with only two beams, the combiner peak injection efficiency is low (Fig. 7), only of order 10%.

Baseline rotation can in principle be accomplished either with a rotating dual aperture mask, or by first passing the telescope beam through a pupil rotator, such as a K-mirror, and then employing a fixed sub-aperture mask. The first option leads to a number of rotating beams after the sub-aperture mask, and so the nulling beamcombiner must be able to deal with lateral beam motion. Only the fiber nulloer seems a natural match to such a contingency, since in this case, both beams are within the broad fiber acceptance cone, and so the baseline between the sub-apertures can have any orientation (i.e. the 2 beams in the fiber nulloer illustrated in Fig. 5 can be rotated about the axis of symmetry of the Figure). This leads to a very simple configuration for the rotating-baseline nulloer, shown as case I in Fig. 8.

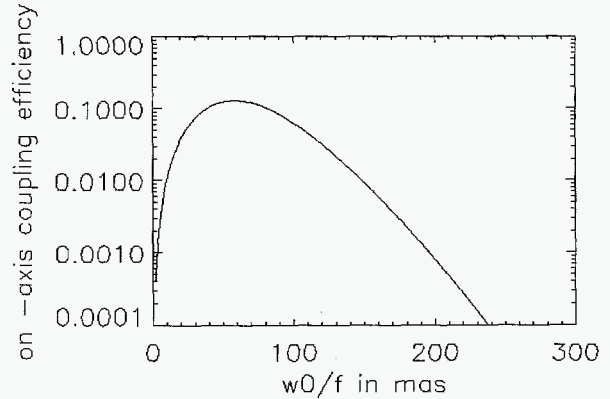


Figure 7. Injection efficiency of a two-beam fiber nulloer, for an on-axis source, for the case of a pair of 1.5 m sub-apertures separated by 3.5 m. The ordinate is  $w_0/f$ , where  $w_0$  is the mode radius and  $f$  is the focal length of the lens illuminating the fiber.

However, in this approach, the achromatic phase shifter would either need to rotate with the sub-aperture mask, or it would be necessary to accept a large dead zone in rotation angle as the sub-apertures transition across the phase step. Neither of these solutions is ideal, but nevertheless, they provide simple and feasible nulling solutions that are also quick to implement. The disadvantage of a rotating phase shifter can be obviated if a pupil rotator, such as a K-mirror, were to be used instead, in which case a fixed dual-aperture mask could define the rotating sub-apertures (Fig. 8, cases IIa and IIb. Case IIa is still a fiber nulloer but case IIb is now a beamsplitter-based nulloer. In such an approach, the selected rotating sub-aperture beams now lie exclusively upstream of the K-mirror, and the downstream nulling optics thus need only accommodate fixed beams. The upstream beams are of course free to rotate within the larger telescope pupil. Of course, such an approach brings the need for an accurate pupil rotator.

While a fiber nulloer can be used with a fixed sub-aperture mask as well (Case IIa), so can more classical beamsplitter-based nulling beamcombiners. Indeed, as indicated by cases IIa and IIb of Fig. 8, any type of nulloer can follow the pupil rotator and the fixed subaperture mask. This provides a high degree of flexibility, as a number of familiar nulling beam-combiner configurations can then be considered, including fiber nulloers, single beamsplitters, and dual-beamsplitter-based configurations such as rotational shearing interferometers, and dual-beam Mach-Zehnder, Sagnac and Michelson interferometers [3]. In the classical beamsplitter-based case, the light from the combined beam can be focused into a fiber with high efficiency, thus avoiding the losses inherent in the fiber nulloer approach.

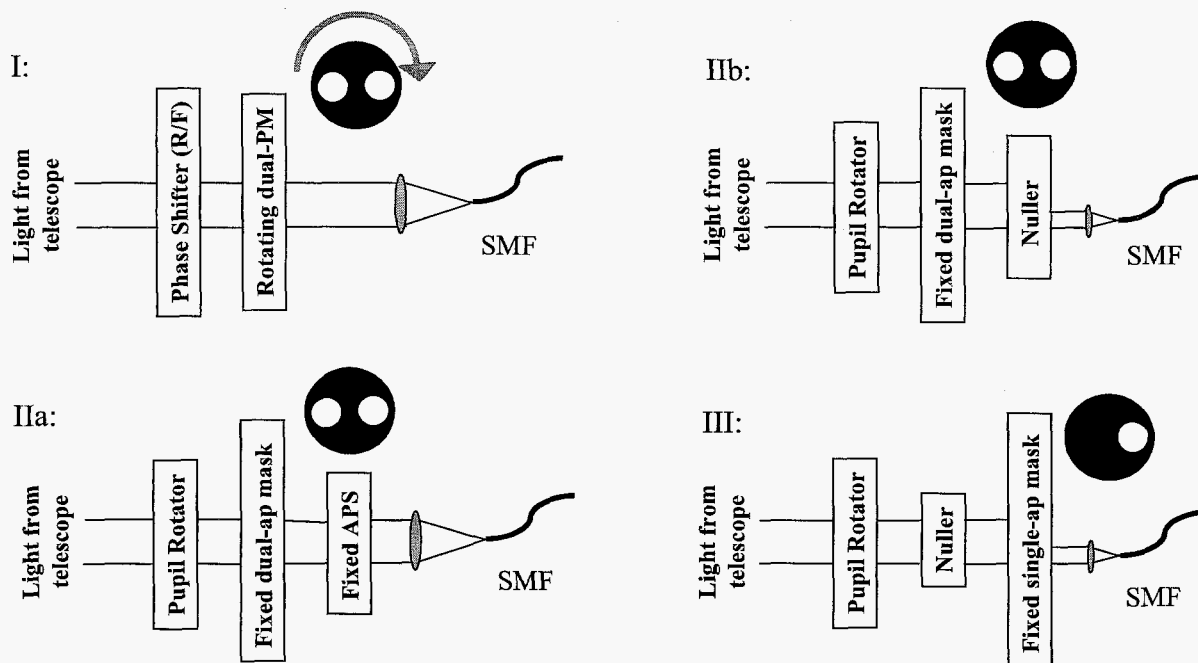


Figure 8. Four potential layouts for a rotating nuller on a single-aperture telescope. R/F means “rotating or fixed”, PM is “pupil mask”, APS is “achromatic phase shifter”, SMF is “single mode filter”, and “ap” is short for “aperture”. In version III, only a single subaperture is necessary, although more subapertures could be used to increase efficiency or to lay out different pupil-plane configurations.

Finally, by reversing the order of the pupil mask and nuller, a single-aperture mask can be used to define both of the pair of sub-apertures, because in reverse propagation, the nulling beamcombiner generates two initial beams out of the one final combined beam. In this configuration, different nulling beamcombiners can also be considered, but one choice which is easy to visualize is a symmetric rotational shearing interferometer (RSI). An RSI, for example, provides several advantages. First, since RSIs combine two pupil images rotated by 180 degrees, all baselines centered on the pupil are generated simultaneously. A number of baselines can then be accessed simultaneously by means of different off-axis subapertures feeding different fibers, thus achieving pupil efficiencies approaching unity. Second, each baseline is duplicated on the opposite side of the center in the recombined pupil. This duplicate baseline can be made use of for e.g., a second waveband, or for phase measurement and control. Other nulling beam-combiner configurations, such as dual-beam Mach-Zehnder or Sagnac interferometers, can also be used, with a similar, but not identical, set of advantages. Clearly, a wide range of nulling beamcombiner configurations can be employed with a rotating nuller.

#### 4. BASIC PERFORMANCE

How well might a rotating sub-aperture nuller on a large ground-based telescope perform? The main questions are the inner working distance (IWD), i.e., the smallest angular offset at which a companion can be detected, the achievable contrast vs. radial offset, and the sensitivity loss due to the collecting area reduction. The last point is illustrated in Fig. 7 for the fiber nuller, where a roughly 10% peak transmission is seen. For beamsplitter-based combiners, the loss is smaller, being given by the summed sub-aperture area fraction. The IWD is given by  $IWD = \alpha\lambda/2b$ , where  $\lambda$  is the wavelength,  $b$  the baseline length,  $\lambda/2b$  is the angular offset to the first constructive fringe peak, and  $\alpha$  is a constant of order unity. There is a certain freedom in determining  $\alpha$ , and different potential choices range from e.g., the fringe half-power point,  $\alpha = 0.5$ , to just under unity ( $\alpha \approx 0.85$ ) if the central-most region where off-axis companions start to undergo cancellation is to be avoided. This latter point is illustrated in Fig. 9, where it can be seen that at large angles the reconstructed image tracks the off-axis companion position, while in the central-most region, the residual source leakage gets “stuck” at a relatively fixed radial offset outside of the central cancellation region.

Even so, since the maximum baseline length available within the single aperture telescope pupil is  $D - s$ , where  $D$  is the aperture diameter and  $s$  the sub-aperture diameter, we have  $IWD = \alpha\lambda/(2(D-s))$ . If we take  $s=D/3$  to avoid the central obscuration, we get  $IWD = 0.75\alpha\lambda/D$ . Thus, independent of the exact value of  $\alpha$ , the IWD is significantly smaller ( $\approx 0.5\lambda/D$ ) than that of a classical coronagraph (several  $\lambda/D$ ), and so a rotating nuller using only part of the full pupil can in principle be used for observations closer to the optical axis than a classical coronagraph utilizing the full telescope pupil.

On the other hand, the diameter of the field of view, FOV, is set by the width of the subaperture beam coupling to the single mode fiber. A smaller sub-aperture comes with an increased FOV, since  $FOV \approx \lambda/s$ . In general,  $FOV/IWD = 2(D-s)/(\alpha s)$ . For  $s = D/3$ , the case discussed earlier,  $FOV \approx 3\lambda/D$ , and  $FOV/IWD = 4/\alpha$ . The accessible angles are thus restricted by the finite FOV, but they cover a range otherwise inaccessible, and so very useful, at small radial offsets from the center.

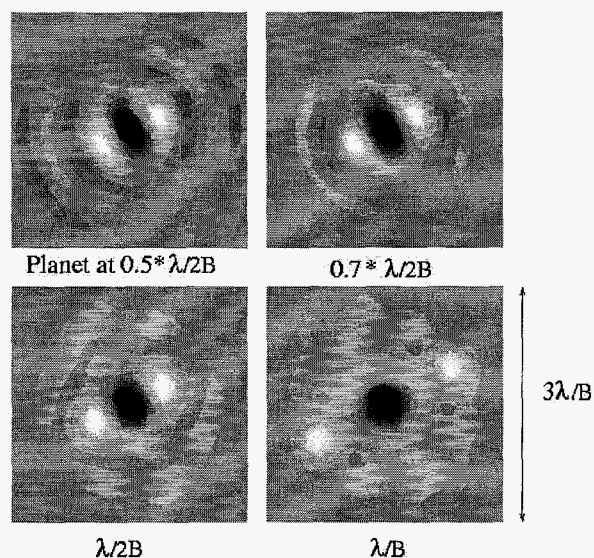


Figure 9. Reconstructed images for a single off-axis point source at a range of off-axis offsets. At large angular offsets, the reconstructed image tracks the input source position, but for a source inside of  $\lambda/2b$ , the source position is not reproduced well, as the residual flux remains pinned outside of the central region of cancellation.

The attainable null depth,  $N$ , will be limited mainly by the phase offset,  $\phi$ , between the two subapertures, and is given by  $N = (\phi/2)^2$ . For small  $\phi$ , the expected null depth can be estimated from the root-mean-square phase across the aperture. This is obtainable from the Strehl ratio,  $S$ , in a “worst case” sense, by means of the small-angle relation  $S = 1 - \phi^2$ . Thus,  $N \approx (1-S)/4$ . For a typical current-generation

adaptive optics (AO) system, with  $S \approx 0.6$  at K-band (2.2  $\mu\text{m}$ ), corresponding to  $\phi \approx 200$  nm, the average null is thus expected to be  $\approx 0.1$ . However, path length fluctuations will lead to null depths that occasionally reach much deeper levels over short integration times, and so the interesting quantity is the lower envelope of the null depth fluctuations, as a function of rotation angle.

The detailed performance expected with such a basic sub-aperture nuller behind a current-generation AO system, with no further phase correction, is shown in Figure 10. These simulations of instantaneous null depth reproduce the expected 0.1 average null level discussed above (the upper envelope of the traces), and also show that even without further phase correction, off-axis sources can be detected by means of their effect on the lower envelope of the null depth fluctuations. At each rotation angle of the baseline, one simply measures the null fluctuations over a long enough time interval for the lower envelope of the fluctuations to show the expected variations.

## 5. IMPROVED PERFORMANCE

There are a number of ways to provide improved performance. First, with potential next generation AO systems, improvements in Strehl ratios to  $\approx 0.95$  and rms phases to  $\approx 75$  nm are foreseen. With a rotating sub-aperture nuller, the uncorrected average null level, i.e., the upper envelope of the curves in Figure 10, can then be expected to drop to as low as  $\approx 0.01$ , improving expected performance by an order of magnitude. Note that this level of AO performance has recently been demonstrated using a well-corrected sub-aperture at Palomar [8], and so this level of nulling performance can actually already be achieved with present capabilities, if the nulling baseline lies within a well-corrected sub-aperture, at the cost of further baseline and SNR reductions. However, it is important to point out that a rejection of 100:1 is already useful in the study of very close binary stars.

On the other hand, a more active method of improving performance is to provide a greater degree of phase control between the sub-apertures, because the null depth is limited by the fluctuations in relative phase between the sub-apertures. An accurate measurement of this phase difference, and correction for it, can thus directly improve the null stability. Because of the large size of potential off-axis sub-apertures (a few meters on large ground-based telescopes), the SNR of such a measurement will be much higher than is possible with the typically small AO correction cell sizes (a few tens of cm). Thus, with such a second layer of phase correction between the sub-apertures, significant improvement in the null depth stability can be achieved, allowing more reliable measurement of deeper null levels.

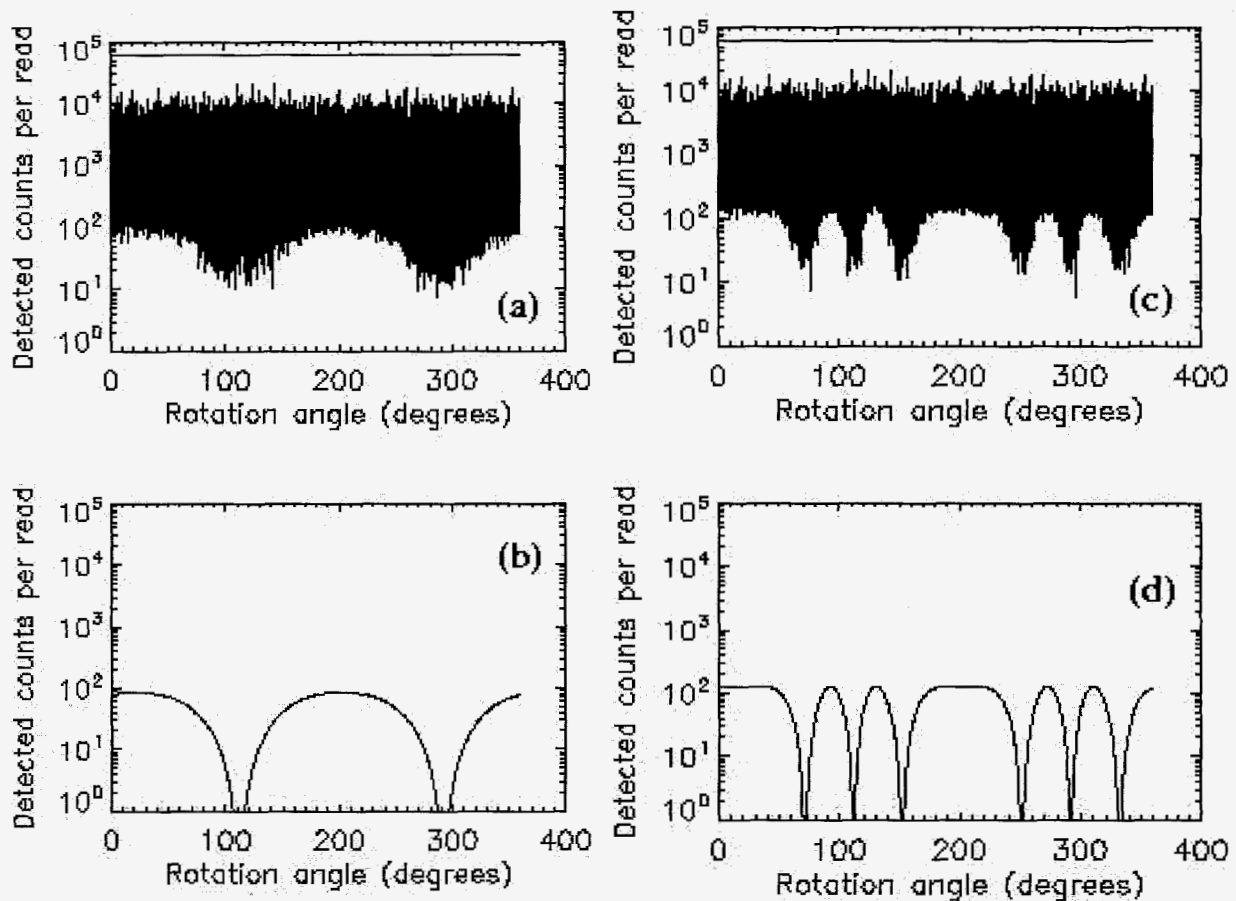


Figure 10. Expected performance of a rotating sub-aperture fiber nuller on the Palomar 200 inch telescope in K band, without any phase stabilization beyond that provided by the Palomar AO system (assuming a Strehl ratio of 70% over the full aperture). The assumed geometry is a pair of 1.5 m diameter subapertures on a baseline of 3.5 m. Panels b and d show the theoretical companion signal vs. rotation angle for a pair of binaries of contrast ratio 500, with separations of 40 mas and 200 mas, respectively. Only the signals from the fainter secondaries are shown, and the primaries are assumed to have  $m_K = 3$ . Panels a and c show simulations of the expected signals measured for 100 baseline rotations, assuming 1000 reads of 10 ms per turn. Both background and read noise ( $10e^-$ ) are included. The constructive state is indicated by the horizontal lines in panels a and c. For stellar rejections of up to about 10,000:1, the bottom envelope of the null depth fluctuations follows the theoretically expected curves. With an extra layer of phase stabilization between the subapertures, or a next generation AO system, the performance improves as discussed in the text.

In particular, given the large photon fluxes available in the near-infrared, the timescale for collecting enough photons for the phase measurement can be quite short. The accuracy of a phase measurement is given by the familiar formula,  $\phi \approx 1/\text{SNR}$ , where small factors of order unity have been ignored. In the signal-dominated case, the SNR is the square root of the number of detected stellar photons per measurement cycle, which is given by  $Rt$ , where  $R$  is the detection rate and  $t$  the integration time. Since the null depth is given by the square of half the phase error (Section 4), the attainable null depth,  $N$ , is inversely proportional to the detection rate of incident stellar photons. Allowing for phase measurements at a wavelength half that of the nulling band (e.g., J-band vs. K band), the result is that  $t =$

$1/(16R_jN)$ . Thus even allowing for a J-band transmission of order 0.1, the phase accuracy needed to maintain a null of order  $10^{-4}$  can be obtained on a 5<sup>th</sup> magnitude star in a time of order  $10^{-4}$  sec, well below atmospheric coherence timescales.

Indeed, in interferometers with multiple outputs, the phase measurement can become fairly straightforward. For example, because dual copies of any baseline are available in an RSI, one of the dual outputs can be used to measure and stabilize the phase of the second output, which is held fixed at null. Additional SNR improvements are also possible, by means of the inclusion of additional output ports sampling different baseline lengths. In particular,

source reconstruction would be eased by the addition of output sub-apertures covering a range of baseline lengths (e.g., Fig. 11).

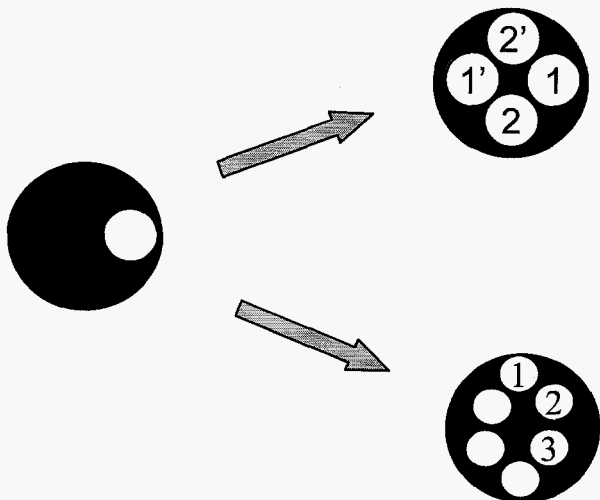


Figure 11. Potential performance improvement in both SNR and phase stability can be achieved by means of extra subapertures in the pupil plane. The top right pupil allows phase control of the un-primed outputs by means of the primed outputs. However, the selected baseline length is also duplicated at a  $90^\circ$  rotation angles, to increase the SNR. The bottom right pupil also allows for different baseline lengths, to allow a better sampling of the source structure.

## 6. THE ROLE OF THE SPATIAL FILTER

It is important to emphasize the key role that the final spatial filter plays. For both linear and rotational shearing interferometers, tip-tilt errors degrade the central stellar null with a  $\theta^2$  dependence. In contrast, if a single-mode fiber is used to spatially filter the focal plane field, tip-tilt errors do not have as large an impact. In this case, tip-tilt errors affect the coupling of the starlight to the fiber, and so are translated into intensity changes. This converts the null sensitivity to a  $\theta^4$  dependence. This was discussed in [9], but can be easily seen to be the case from the basic transmission properties of single-mode fibers, which only allow the propagation of fields oriented perpendicular to the propagation direction. For a field incident at angle  $\theta$ , the  $\sin\theta$  component along the axis of the fiber thus cannot propagate, because that field component is parallel to the fiber axis. Therefore, the linear residual field component, which would lead to a  $\theta^2$  intensity leakage term, cannot propagate in the fiber. On the other hand, the perpendicular field component, which goes as  $\cos\theta$ , can propagate in the fiber, which leads to a field leakage of  $1-\cos\theta$ . For small  $\theta$ ,

the residual power leakage is then proportional to  $\theta^4$ . Therefore, in the presence of a given level of tip-tilt errors, a single-mode fiber spatial filter in the focal plane is able to provide a much more stable, and hence deeper, level of starlight rejection.

In addition, it is primarily because of the single-mode fiber that one needs only to measure the single phase offset between the two sub-aperture beams to achieve improved nulls. In detail, the fiber erases the sub-pupil tip-tilt residuals, leaving on-axis propagation. Thus, the only phase-related quantity that survives propagation through the fiber is the average phase offset between the two incident fields. The fiber thus also greatly simplifies control issues, by reducing the number of control parameters to a single relative phase, and so provides for a much more robust measurement approach.

## 7. SUMMARY

Rotating space-based nulling interferometers will not only involve many new technologies, but also new signal measurement approaches and image reconstruction techniques. As such, it is highly desirable to test these approaches prior to the launch of any multi-aperture interferometric nuller. One way to test potential signal measurement and reconstruction approaches is with a rotating sub-aperture nuller operating within the pupil of a single ground-based telescope, as we describe here in detail. However, in addition to simply testing interferometric approaches, it turns out that such a rotating nuller will also provide a very capable coronagraph, with a high dynamic range and a small inner working angle, thus providing a scientific justification for building and using such a device on an existing ground-based telescope. The potential for novel scientific observations at small inner working angles will be essential to obtain the observing time needed on ground-based telescopes to test these ideas.

The needed nulling coronagraph can be implemented in a number of ways, from a simple rotating pupil mask with a fiber combiner, to more complex and capable systems which begin with a pupil rotator, and are followed with any type of nuller. The expected performance depends heavily on the level of phase correction, but even with the simplest approach, that of passively relying on an existing AO system, the approach can begin to be validated with observations of binary stars of low contrast. In fact, with improvements expected with next generation AO systems, an order of magnitude performance improvement is predicted. On the other hand, inclusion of phase measurement and correction between the sub-apertures can provide the control level needed to obtain stable nulls at the  $10^{-3}$  to  $10^{-4}$  level in the  $2\ \mu\text{m}$  K-band. With this level of performance, the signal extraction and image reconstruction approaches being considered for space based nulling

interferometers can be tested under real astronomical observing conditions, thus providing a level of confidence in the rotating nulling interferometer approach which is lacking at the present time

extensive experience in astronomical nulling and single-mode interferometry.

This work was carried out at the Jet Propulsion Laboratory, California Institute of Technology, under contract with the National Aeronautics and Space Administration

## REFERENCES

- [1] J.R.P. Angel and N.J. Woolf 1997, "An imaging nulling interferometer to study extrasolar planets," *Astrophys. J.* 475, 373
- [2] R.N. Bracewell 1978, "Detecting nonsolar planets by spinning infrared interferometer," *Nature* 274, 780.
- [3] E. Serabyn 2003, "Nulling Interferometry Progress," in *Proc. SPIE* 4838, 594
- [4] V. Weber et al. 2004, "Nulling interferometer based on an integrated optics combiner," in *Proc. SPIE* 5491, 842
- [5] O. Wallner, J.M.P. Armengol and A. Karlsson 2004, "Multi-axial single-mode beam combiner," in *Proc. SPIE* 5491, 798
- [6] P. Haguenaer and E. Serabyn, 2006, *Applied Optics*, in press.
- [7] R. Angel 1989, "Use of a 16m telescope to detect earthlike planets," in "The Next Generation Space Telescope," STScI, p. 81
- [8] P. Haguenaer et al. 2005, "An off-axis four-quadrant phase mask coronagraph for Palomar," in *Proc SPIE* 5905, 59050S-1
- [9] B. Mennesson et al. 2002, *JOSA* 19, 596

## BIOGRAPHY

**Gene Serabyn** is a Senior Research Scientist at the Jet Propulsion Laboratory, where he serves as the Keck Interferometer Nulling Scientist, and the TPF Interferometer Scientist. He has a BS in Physics from MIT and a PhD in Physics from UC Berkeley. He has worked on a number of novel astronomical instruments at a variety of wavelengths.

**Bertrand Mennesson** is a Senior Staff Member at the Jet Propulsion Laboratory, where he serves as the TPF Deputy Interferometer Scientist. He has a MS and PhD in Astrophysics from the Observatory of Paris, and has